12-21-2014

Satellite evidence for significant biophysical consequences of the "Grain for Green" Program on the Loess Plateau in China

Jingfeng Xiao
University of New Hampshire, Durham, j.xiao@unh.edu

Recommended Citation
Xiao, J. (2014). Satellite evidence for significant biophysical consequences of the "Grain for Green" Program on the Loess Plateau in China. Journal of Geophysical Research: Biogeosciences, 119, 2261–2275, https://dx.doi.org/10.1002/2014JG002820. (Paper featured on the cover of the journal).

AGU PUBLICATIONS

JGR

Journal of Geophysical Research: Biogeosciences

RESEARCH ARTICLE
10.1002/2014JG002820

Key Points:
- The Grain for Green Program increased forest cover of the Loess Plateau in China
- The GGP alters carbon cycling, hydrological processes, and surface energy exchange
- Large-scale afforestation has significant feedbacks to the regional climate

Correspondence to:
J. Xiao,
j.xiao@unh.edu.

Citation:
Xiao, J. (2014), Satellite evidence for significant biophysical consequences of the "Grain for Green" Program on the Loess Plateau in China, *J. Geophys. Res. Biogeosci.*, *119*, 2261–2275, doi:10.1002/2014JG002820.

Received 6 OCT 2014
Accepted 19 NOV 2014
Accepted article online 21 NOV 2014
Published online 21 DEC 2014

Satellite evidence for significant biophysical consequences of the "Grain for Green" Program on the Loess Plateau in China

Jingfeng Xiao[1,2]

[1]International Center for Ecology, Meteorology, and Environment, School of Applied Meteorology, Nanjing University of Information Science and Technology, Nanjing, Jiangsu, China, [2]Earth Systems Research Center, Institute for the Study of Earth, Oceans, and Space, University of New Hampshire, Durham, New Hampshire, USA

Abstract Afforestation has been implemented worldwide as regional and national policies to address environmental problems and to improve ecosystem services. China's central government launched the "Grain for Green" Program (GGP) in 1999 to increase forest cover and to control soil erosion by converting agricultural lands on steep slopes to forests and grasslands. Here a variety of satellite data products from the Moderate Resolution Imaging Spectroradiometer were used to assess the biophysical consequences of the GGP for the Loess Plateau, the pilot region of the program. The average tree cover of the plateau substantially increased because of the GGP, with a relative increase of 41.0%. The GGP led to significant increases in enhanced vegetation index (EVI), leaf area index, and the fraction of photosynthetically active radiation absorbed by canopies. The increase in forest productivity as approximated by EVI was not driven by elevated air temperature, changing precipitation, or rising atmospheric carbon dioxide concentrations. Moreover, the afforestation significantly reduced surface albedo, leading to a positive radiative forcing and a warming effect on the climate. The GGP also led to a significant decline in daytime land surface temperature and exerted a cooling effect on the climate. The GGP therefore has significant biophysical consequences by altering carbon cycling, hydrologic processes, and surface energy exchange and has significant feedbacks to the regional climate. The net radiative forcing on the climate depends on the offsetting of the negative forcing from carbon sequestration and higher evapotranspiration and the positive forcing from lower albedo.

1. Introduction

Afforestation has been implemented worldwide as regional and national policies to sequester carbon dioxide (CO_2) from the atmosphere [*Pan et al.*, 2011], control soil erosion [*Deng et al.*, 2012], and improve water quality and restore other ecosystem services [*Sun et al.*, 2006]. Afforestation and reforestation have been nationwide efforts in China since the early 1950s. According to the national forest inventories, the persistent, nationwide efforts on forest plantations increased total forest area from 1.22×10^6 km^2 in the middle 1970s to 1.95×10^6 km^2 in circa 2006 (2004–2008) with an increase of 60.0% [*State Forestry Administration of China*, 1977, 2009a]. Today, China has the largest area of forest plantations in the world with 6.2×10^5 km^2 (or 62.0×10^6 ha), accounting for 31.8% of the total forested land [*State Forestry Administration of China*, 2009a]. The conversion of grasslands, croplands, or shrublands to forests can alter the carbon cycling, hydrological processes, and surface energy exchange and have potentially significant feedbacks to the local and regional climate [*Bonan*, 2008; *Y. Q. Liu et al.*, 2008].

The Loess Plateau of China occupies ~6.4×10^5 km^2 of land in the middle reaches of the Yellow River and is known as the cradle of the ancient Chinese civilization. The plateau was well covered by trees and grasses until the Western Han Dynasty (206 B.C. to 8 A.D.) [*Fang and Xie*, 1994]. However, due to deforestation it now has serious ecological and environmental problems. The long-term deforestation has been driven mainly by human activities and partly by climate change [*Fang and Xie*, 1994]. The widespread deforestation led to intensive soil erosion [*Zheng*, 2006]. The Loess Plateau is well known for its intensive soil erosion, contributing ~90% of the sediments in the Yellow River [*Ren and Shi*, 1986]. The soil erosion also caused substantial loss of nutrients (e.g., organic matter, nitrogen, and phosphorus) [*Zheng et al.*, 2005], leading to lower plant productivity and crop yield.

China's central government has implemented a series of national policies to address pressing environmental problems and to improve ecosystem services in northwestern and northern China including the Loess Plateau. These policies include the "Three-North Belt" Program, grassland restoration and conservation, and the "Grain for Green" Program (GGP). The GGP was launched in 1999, and its goals are to increase forest cover and to mitigate soil erosion by converting agricultural lands on steep slopes to forests and grasslands. These agricultural lands are typically characterized by low productivity and intensive soil erosion. The famers with loss of croplands are subsidized by grain and cash subsidies for up to 8 years. The GGP is expected to increase forest cover, enhance carbon sequestration, control soil and water loss, and reduce dust to other regions and countries [*J. G. Liu et al*., 2008]. The Loess Plateau is the pilot region of the GGP.

The conversion of croplands to forests can alter plant productivity and ecosystem carbon fluxes. Forests can have higher gross primary productivity (GPP) and net ecosystem productivity than croplands [*Xiao et al*., 2013]. Forest plantations can significantly sequester carbon by storing carbon in biomass and soils. Previous studies have shown that the conversions of farmlands to forests and grasslands increased net primary productivity (NPP) and soil carbon storage [*Chang et al*., 2011; *Lu et al*., 2012; *Su and Fu*, 2013; *Liu et al*., 2014]. Forests can also have higher evapotranspiration (ET) than croplands [*Xiao et al*., 2013]. The large-scale conversion of croplands to forests can potentially alter the hydrological processes and latent heat fluxes at regional scales. However, there has been little regional-scale evidence on the GGP-induced increases in forest cover and the subsequent ecological consequences from satellite or field observations.

The conversion of croplands to forests can also alter land surface albedo. Albedo is the fraction of incident solar radiation (0.3–5.0 μm) reflected by the land surface. It is an important parameter in climate models, numerical weather models, and surface energy budget studies [*Dickinson*, 1995]. Forests have lower albedo than croplands. Afforestation can lead to decreases in albedo, which can contribute to planetary warming through increased solar heating of the land surface [*Bonan*, 2008]. Large-scale conversions of croplands to forests because of the GGP can therefore potentially alter land surface albedo of the Loess Plateau and the amount of solar radiation absorbed in the regional climate system.

Satellite remote sensing provides a viable means for quantifying dynamics of vegetation cover [*Hansen et al*., 2010] and plant productivity [*Xiao and Moody*, 2004] and for assessing the resulting effects on biophysical properties and the surface energy exchange [*Lyons et al*., 2008] at broad scales. The Moderate Resolution Imaging Spectroradiometer (MODIS) sensors on board the Terra and the follow-up platform Aqua have been providing global coverage of the land surface within 1–2 days since late February 2000 [*Justice et al*., 2002]. To date, we have access to 14 years of MODIS observations. These MODIS observations are potentially valuable for assessing the changes in tree cover resulting from the GGP and the resulting biophysical consequences.

In this study, satellite evidence is presented on the biophysical consequences of the GGP for the Loess Plateau, the pilot region of the program. A variety of MODIS data streams including tree cover, vegetation indices, leaf area index (LAI), photosynthetically active radiation (fPAR) absorbed by vegetation canopies, albedo, and land surface temperature (LST) and forestry statistics were used to quantify the changes in tree cover resulting from the GGP and the biophysical consequences for the Loess Plateau over the period from 2000 to 2013. It has been nearly 15 years since the launch of the program, and it is timely to assess to what extent the GGP alters forest cover and biophysical properties over the Loess Plateau. Assessing the biophysical consequences of the GGP has both scientific and policy implications.

2. Data and Methods

2.1. Study Region

The Loess Plateau occupies 6.4×10^5 km^2 of land in the middle reaches of the Yellow River, accounting for 6.7% of China's land area (Figure 1). The plateau is to the west of the Taihang Mountains and to the east of Helan Mountains, and to the north of Qinling Mountains and to the south of the Great Wall. The plateau consists of the entirety of two provinces (or autonomous regions)—Shanxi and Ningxia—and portions of five provinces (or autonomous regions): Shaanxi, Henan, Inner Mongolia, Gansu, and Qinghai (Figure 1).

The Loess Plateau is characterized by temperate continental monsoon climate with mean annual temperature ranging from 4 to 14°C and mean annual precipitation from 200 to 750 mm [*Su and Fu*, 2013].

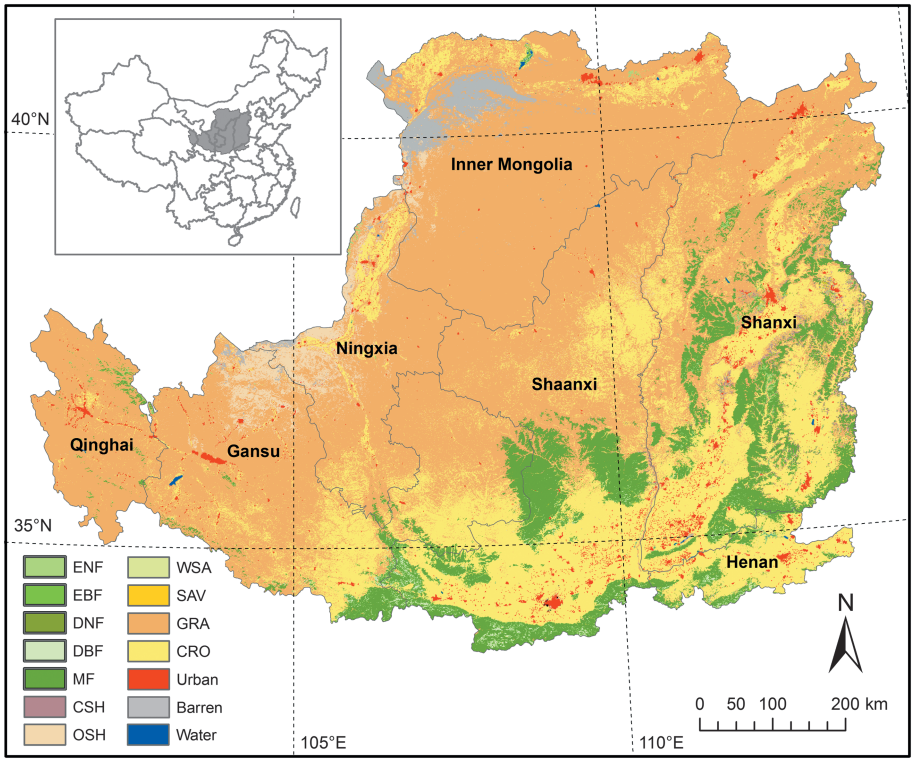

Figure 1. The Loess Plateau region and the distribution of land cover types. The Loess Plateau is composed of the entirety or portions of seven provinces (or autonomous regions): Inner Mongolia, Ningxia, Shaanxi, Shanxi, Gansu, Henan, and Qinghai. The base map is the 500 m MODIS land cover map [*Friedl et al.*, 2010]. The major vegetation types include evergreen needleleaf forests (ENF), evergreen broadleaf forests (EBF), deciduous needleleaf forests (DNF), deciduous broadleaf forests (DBF), mixed forests (MF), closed shrublands (CSH), open shrublands (OSH), woody savannas (WSA), savannas (SAV), grasslands (GRA), and croplands (CRO).

The plateau encompasses three climatic zones: semihumid, semiarid, and arid. Annual precipitation is influenced by the strength of the monsoon and complex topography and varies substantially over space and time. Annual precipitation decreases from the southeast to the northwest. The plateau is dominated by croplands and forests in the southeast and by grasslands, shrublands, and barren land in the northwest. Over the last five decades, annual mean temperature increased by 1.19°C and annual precipitation decreased by 29.1 mm on the plateau [*Wang et al.*, 2012]. Therefore, the Loess Plateau exhibited a warming and drying trend [*Liu et al.*, 2006; *Zhang et al.*, 2012].

2.2. MODIS Data Products

The following data products from the MODIS on board NASA's Terra and Aqua satellites were used in this study: vegetation continuous fields, vegetation indices, GPP, LAI, fPAR, albedo, ET, and LST. The GPP and ET data were obtained from the Numerical Terradynamic Simulation Group, University of Montana (http://www.ntsg.umt.edu), and other products were obtained from NASA's Earth Observing System Data and Information System (EOSDIS; http://reverb.echo.nasa.gov). These data products are summarized in Table 1.

2.2.1. Vegetation Continuous Fields

Tree cover mapping is of growing importance because tree cover is an important variable for biogeochemical [*Liu et al.*, 2014] and land surface modeling [*Lawrence and Chase*, 2007]. Tree cover mapping is also important in the policy arena [*Hansen et al.*, 2002]. There is tremendous interest in quantifying the changes in tree cover resulting from deforestation or afforestation at regional or global scales.

The MODIS Vegetation Continuous Fields (VCFs) product (MOD44B) [*DiMiceli et al.*, 2011] was used to quantify the changes in tree cover. The VCF product is an annual product and provides a subpixel level representation of surface vegetation cover globally. The product is at 250 m spatial resolution and is

Table 1. Summary of the MODIS Data Products Used in This Study

Short Name	MODIS Data Product	Platform	Spatial Resolution	Temporal Resolution	Period
MOD44B	Vegetation Continuous Fields	Terra	250 m	Yearly	2000–2010
MOD13A2	EVI	Terra	250 m	16 day	2000–2013
MOD17A3	GPP	Terra	1 km	Yearly	2001
MOD16A3	ET	Terra	1 km	Yearly	2001
MOD15A2	LAI/fPAR	Terra	1 km	8 day	2000–2013
MCD43A3	Albedo	Terra/Aqua	500 m	16 day	2000–2013
MOD11A2	LST	Terra	1 km	8 day	2000–2013

currently available from 2000 to 2010. It currently only contains the percent tree cover layer. The two additional layers (i.e., percent nontree vegetation and percent bare) will be included in the future. For each 250 m pixel, the VCF product provides the percent tree cover (%) estimate.

2.2.2. Vegetation Indices

The MODIS vegetation index (VI) data product (MOD13A2) [*Huete et al*., 2002] was obtained for the period from 2000 to 2013. This product consists of normalized difference vegetation index (NDVI) and enhanced vegetation index (EVI), both of which are available at 250 m spatial resolution and 16 day intervals. The NDVI captures the contrast between the visible-red and near-infrared reflectance of vegetation canopies. NDVI is closely correlated with fPAR [*Asrar et al*., 1984] and photosynthetic activity [*Xiao and Moody*, 2004]. NDVI saturates in a multilayer closed canopy and is also sensitive to both atmospheric aerosols and soil background [*Huete et al*., 2002]. EVI was developed as an improved vegetation index to account for the limitations of NDVI:

$$\mathrm{EVI} = 2.5\frac{\rho_{\mathrm{nir}} - \rho_{\mathrm{red}}}{\rho_{\mathrm{nir}} + (6\rho_{\mathrm{red}} - 7.5\rho_{\mathrm{blue}}) + 1} \quad (1)$$

where ρ_{nir}, ρ_{red}, and ρ_{blue} are the spectral reflectance at the near-infrared, red, and blue wavelengths, respectively.

The vegetation index product is available as 16 day composites rather than daily images in order to minimize the effects of cloud contamination and to improve the data quality. For a 16 day cycle, a maximum of 64 imagery may be collected because of sensor orbit overlap and multiple observations in a single day; however, due to cloud presence and actual sensor spatial coverage, the actual number of observations ranges from 0 to 64 with fewer observations in the tropics [*Huete et al*., 2002]. The higher-quality, cloud-free, and filtered data are used for compositing. The MODIS-derived EVI was used in this study.

2.2.3. GPP and ET

The MODIS GPP (MOD17A3) and ET (MOD16A3) were used in this study to illustrate the differences in GPP and ET among vegetation types. The MODIS GPP/NPP data product [*Running et al*., 2004; *Zhao et al*., 2005] is the first continuous satellite-derived data set monitoring global vegetation productivity. The product algorithm is based on Monteith's original logic [*Monteith*, 1972, 1977] that NPP under nonstressed conditions is linearly related to fPAR during the growing season. The MODIS ET product considers both the surface energy partitioning process and environmental constraints on ET and use meteorological data and remote sensing data from MODIS to estimate ET [*Mu et al*., 2007]. Both products are available at 1 km spatial resolution and 8 day time steps. Annual GPP and ET were used in this study.

2.2.4. LAI and fPAR

LAI is typically defined as one-sided green leaf area per unit ground area for broadleaf canopies and as the projected needle leaf area for coniferous canopies [*Myneni et al*., 2002]. LAI and fPAR characterizes canopy functioning and the exchange of water and energy and are key parameters in ecosystem, biogeochemistry, and climate models [*Myneni et al*., 2002]. Both variables are often used as satellite inputs to calculate photosynthesis, ET, and NPP, which, in turn, are used to simulate carbon, water, and energy cycle processes.

The MODIS LAI/fPAR data product (MOD15A2) [*Myneni et al*., 2002] was used to quantify the changes in LAI and fPAR resulting from afforestation. LAI and fPAR were retrieved from the surface reflectance from MODIS aboard the TERRA platform using an algorithm based on the physics of radiative transfer in vegetation canopies [*Myneni et al*., 2002]. The LAI and fPAR data products are available at 1 km spatial resolution and 8 day time intervals.

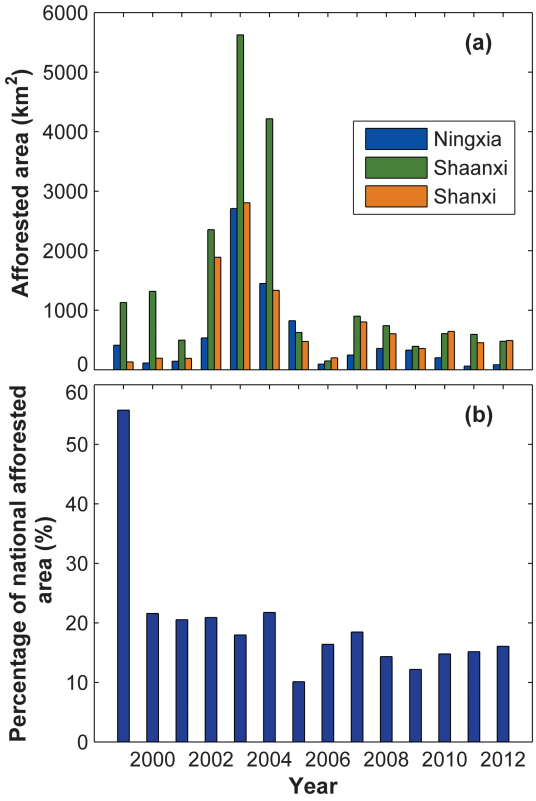

Figure 2. The afforested area resulting from the Grain for Green Program: (a) the annual afforested area (km^2) of three provinces (Shaanxi, Shanxi, and Ningxia) of the Loess Plateau; (b) the proportion (%) that the afforested area of the three provinces accounts for the national afforested area. Other provinces (Inner Mongolia, Gansu, Qinghai, and Henan) are not included in the figure because only small proportions of these provinces are within the extent of the Loess Plateau and the statistics of afforested area are at the provincial level.

2.2.5. Albedo

The MODIS Albedo 16 day L3 Global 500 m product (MCD43A3) was used to quantify the changes in surface albedo resulting from the GGP. This product provides directional hemispherical albedo (black-sky albedo) and bihemispherical albedo (white-sky albedo) [*Schaaf et al*., 2002]. The MODIS bidirectional reflectance distribution function/albedo algorithm is a semiempirical kernel-driven bidirectional reflectance model. Black-sky and white-sky albedo are available at 500 m spatial resolution and 16 day time intervals. The blue-sky albedo under actual atmospheric conditions was calculated as interpolation between the black-sky (direct beam) albedo and white-sky (complete diffuse) albedo as a function of the fraction of diffuse skylight [*Schaaf et al*., 2002].

2.2.6. Land Surface Temperature

The LST derived from MODIS is a measure of the temperature at the land surface. LST integrates the effects of surface-atmosphere interactions and energy fluxes between the atmosphere and the land surface and is one of the key parameters in the physics of land surface processes at regional scales [*Wan et al*., 2002]. LST measures the surface temperature of soils for bare soils and the surface temperature of canopies in densely vegetated areas. For sparsely vegetated areas or mixed pixels with vegetation and bare soils, LST represents the mixed signal of the surface temperature from bare soils and canopies.

The Land Surface Temperature and Emissivity 8 Day L3 Global 1 km product (MOD11A2) was used in this study. LST was retrieved from two thermal-infrared MODIS bands (bands 31 and 32) using the generalized split-window algorithm [*Wan et al*., 2002]. This product is available at 1 km spatial resolution and 8 day time intervals. The MODIS LST agreed with in situ measured LST fairly well, and the discrepancy is within 1 K [*Wan et al*., 2002]. MOD11A2 consists of daytime and nighttime LST, both of which were used in this study.

2.3. Climate Data

Air temperature and precipitation data were obtained from the Modern Era Retrospective-Analysis for Research and Applications (MERRA) reanalysis data set [*Rienecker et al*., 2011]. The MERRA data set is available from the Global Modeling and Assimilation Office (http://gmao.gsfc.nasa.gov/). The data set is at 0.5° × 0.667° spatial resolution and is available in subdaily (every 6 h), daily, and monthly time steps. The temporal coverage of MERRA is from the period 1979 to 2013 that covers the modern era of remotely sensed data, and it makes use of observations from NASA's Earth Observing System satellites. MERRA has improved the representation of the water cycle in reanalysis and has reduced the uncertainty in precipitation [*Rienecker et al*., 2011].

2.4. Forestry Statistics

The afforested area resulting from the GGP was obtained from the China Forestry Statistics Yearbooks for each year over the period from 1999 to 2012 [*State Forestry Administration of China*, 2000–2008, 2009b, 2010–2013] for each province of the Loess Plateau and the entire nation. These statistics summarize the

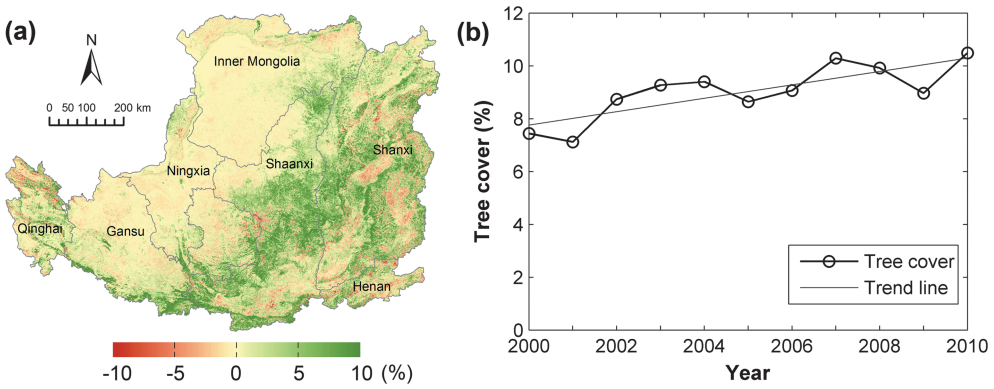

Figure 3. Trends of percent tree cover for the Loess Plateau over the period 2000–2010: (a) trends of percent tree cover on a per pixel basis and (b) trends of percent tree cover averaged across the plateau. The trends in Figure 3a are provided as increases in percent tree cover (%) over the 11 year period.

annual afforested area resulting from the GGP for each province. These provincial statistics do not provide information on the specific locations and distribution within each province.

2.5. Data Analysis

The MODIS data products contain quality assurance (QA) flags that provide information on the quality of the variable for each individual pixel. The QA flags were used to determine the quality of the variable for each pixel. For each variable, the bad value of a given pixel was replaced with good values of the nearest composites using an interpolation approach [*Xiao et al*., 2008; *Zhao et al*., 2005].

For EVI, the 16 day composites from April to September were summed to calculate growing season integrated EVI. The integrated EVI (or NDVI) over the growing season has been widely used as a proxy for plant productivity [*Sims et al*., 2006; *Xiao and Moody*, 2005; *Zhou et al*., 2001]. The spatially averaged EVI time series was produced by averaging growing season EVI across the study region for each year. Similarly, the spatially averaged percent tree cover time series was produced by averaging percent tree cover across the region for each year. The average LAI, fPAR, albedo, daytime LST, and nighttime LST over the growing season were calculated for each pixel for each year. The distributions of EVI, GPP, LAI, fPAR, albedo, ET, daytime LST, and nighttime LST in 2001 were compared among vegetation types using box plots. A box plot provides a useful graphical summary of the distribution of a data set: the central mark of each box is the median, the bottom and top edges of the box are the 25th and 75th percentiles, the whiskers are the maximum and minimum values (i.e., most extreme data points that are not considered as outliers), and outliers are plotted individually beyond the whiskers. The differences in these biophysical properties between forests and croplands were tested using one-way ANOVA. The spatially averaged time series were also produced for these variables. For each pixel, the daily temperature and precipitation data were aggregated to the annual scale to calculate annual mean temperature and annual precipitation for each year. The annual climate data were then averaged across the plateau to produce spatially averaged time series.

The linear trend of percent tree cover was assessed on a per pixel basis and was determined by linearly regressing percent tree cover as a function of time [*Xiao and Moody* 2005; *Zhou et al*., 2001]. The linear trend was also examined for the spatially averaged tree cover time series. Similarly, the linear trends were analyzed for other biophysical variables (EVI, LAI, fPAR, albedo, daytime LST, or nighttime LST).

The correlations of spatially averaged EVI with spatially averaged percent tree cover, air temperature, and precipitation were conducted to examine the influence of climate and afforestation on vegetation productivity. The correlations between EVI and atmospheric carbon dioxide (CO_2) concentrations were also analyzed. Two variables can be correlated with each other simply because they change in the same direction, leading to "spurious correlation." Therefore, for the correlation of two time series, both time series were detrended prior to the correlation analysis to avoid spurious correlation if both time series exhibited increasing or decreasing trends.

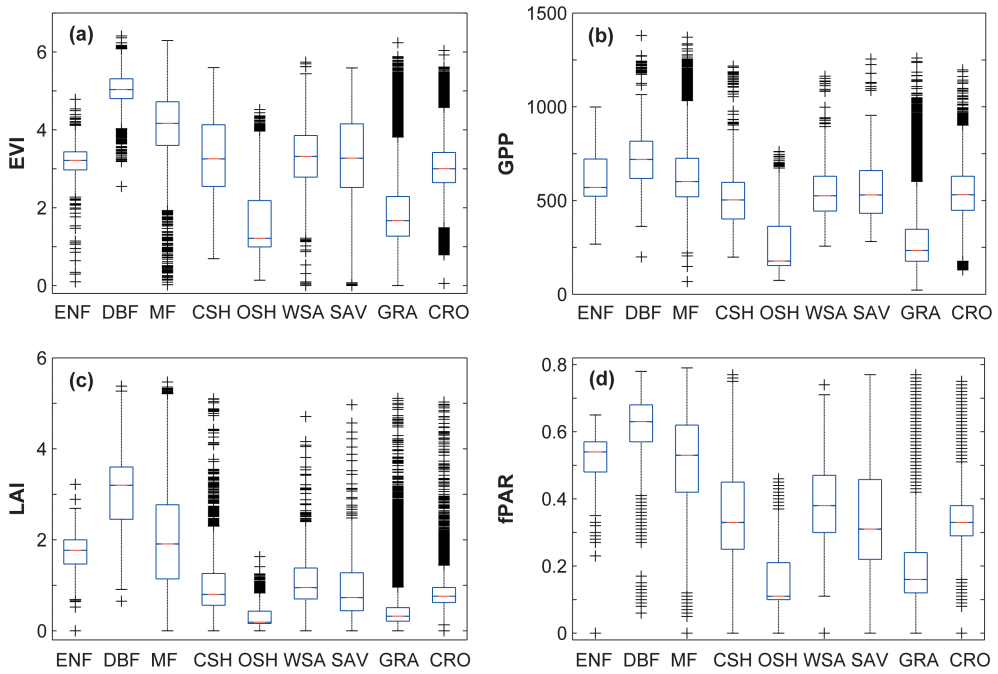

Figure 4. Box plots of per pixel EVI, GPP, LAI, and fPAR on the Loess Plateau in 2001: (a) growing season integrated EVI; (b) annual GPP (g C m^{-2} yr^{-1}); (c) growing season mean LAI; (d) growing season mean fPAR. The abbreviations for the vegetation types are spelled out in the caption of Figure 1.

3. Results

3.1. Increases in Tree Cover

The forestry statistics showed significant conversions of croplands to forests over the Loess Plateau resulting from the GGP. For example, the afforested area of Ningxia, Shaanxi, or Shanxi resulting from the GGP generally ranged from 200 to 1000 km^2/yr, with particularly high areas for 2002, 2003, and 2004 (Figure 2). In 2003, the annual afforested area of Ningxia and Shanxi both reached nearly 3000 km^2, while over 5500 km^2 of cropland was converted to forests in Shaanxi (Figure 2). Altogether, the three provinces accounted for 15–20% of the national afforested area resulting from the GGP for most years, and in 1999, the afforested area of the three provinces accounted for 55.7% of the national afforested area (Figure 2). The total afforested area of the three provinces from 1999 to 2012 reached 3.8×10^4 km^2, accounting for 11.2% of the land area of the three provinces.

The changes in the MODIS-derived percent tree cover (%) over the period 2000–2010 varied over space (Figure 3a). Large increases in tree cover (~5–10%) occurred in eastern, southeastern, and southern Loess Plateau including Shanxi, Shaanxi, and Henan where are dominated by croplands and forests. The remaining areas of the plateau (portions of Ningxia, Inner Mongolia, and Gansu) had small increases or no changes in tree cover. The majority of Ningxia, Inner Mongolia, and Gansu within the Loess Plateau did not exhibit significant changes in tree cover. A tiny portion of the study region had decreases in tree cover.

The average tree cover of the plateau exhibited an increasing trend over the period from 2000 to 2010 (Figure 3b; $y = 0.25x - 499.51$, $R^2 = 0.64$, $p < 0.01$). The average tree cover of the plateau increased from 7.44% to 10.49% from 2000 to 2010, with a relative increase of 41.0%. As a result, the total tree cover derived from MODIS increased from 4.62×10^4 km^2 to 6.51×10^4 km^2 over the Loess Plateau during the 11 year period with an increase of 1.89×10^4 km^2.

3.2. Increases in EVI, LAI, and fPAR

The distributions of per pixel EVI, GPP, LAI, and fPAR in 2001 for each vegetation type were summarized in Figure 4. Among all the vegetation types, deciduous broadleaf forests and mixed forests had the highest EVI (Figure 4a). Each forest type (evergreen needleleaf forests, deciduous broadleaf forests, or mixed forests) had significantly higher EVI than croplands ($p < 0.0001$). Similarly, forests had the highest annual GPP, and each

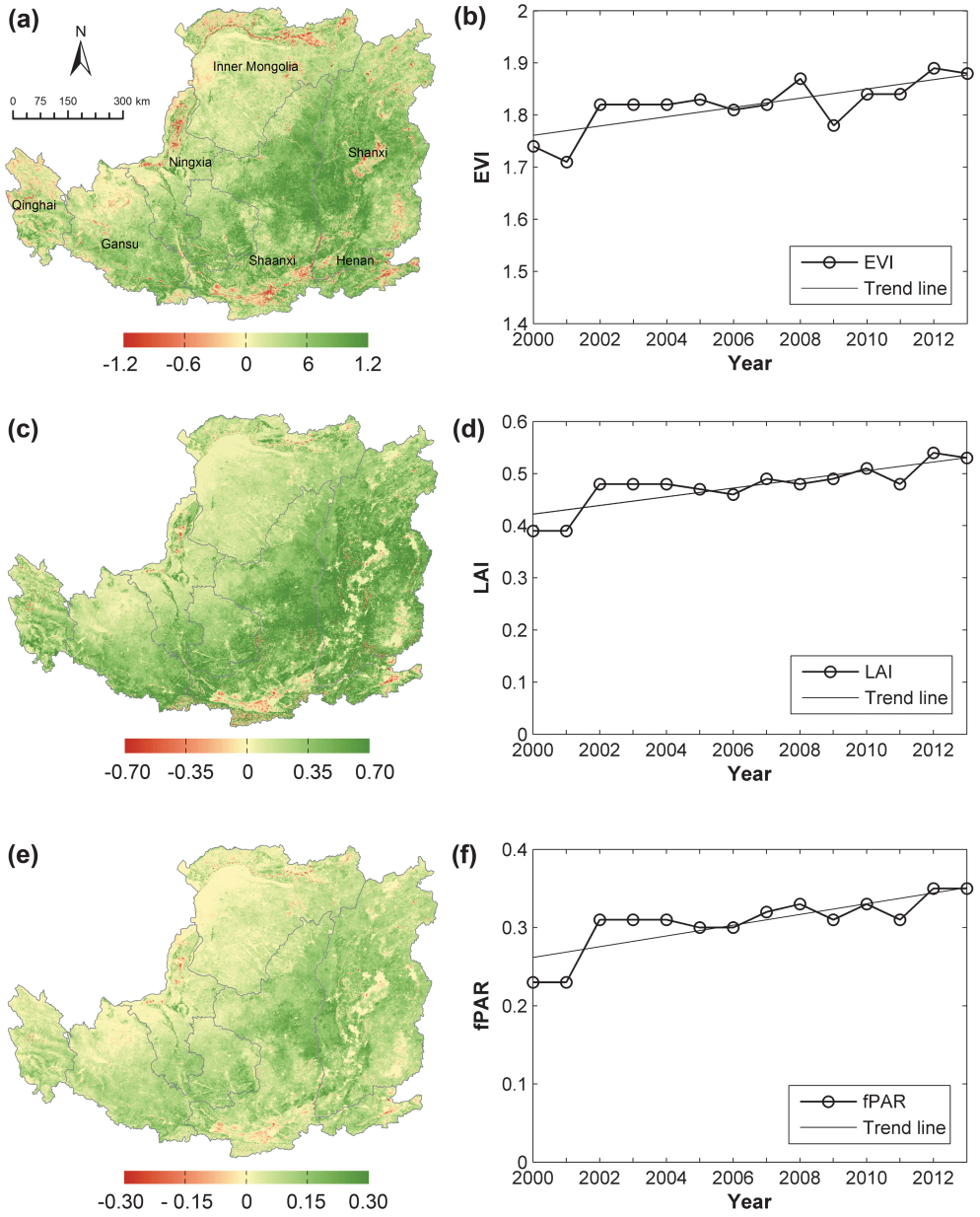

Figure 5. Trends of growing season integrated EVI, mean LAI, and mean fPAR of the Loess Plateau over the period 2000–2013: (a, c, and e) the trends of EVI, LAI, and fPAR on a per pixel basis; (b, d, and f) the trends of EVI, LAI, and fPAR averaged across the plateau. The trends in Figures 5a, 5c, and 5e are provided as increases in EVI, LAI, and fPAR over the 14 year period.

forest type had significantly higher GPP than croplands ($p < 0.0001$) (Figure 4b). Each forest type also had significantly higher LAI ($p < 0.0001$) and fPAR ($p < 0.0001$) than croplands (Figures 4c and 4d). This indicates that the conversion of croplands to forests resulting from the GGP can lead to increases in EVI, GPP, LAI, and fPAR.

The EVI integrated over the growing season exhibited an increasing trend in eastern, southeastern, and southern Loess Plateau, including Shanxi, Shaanxi, and Henan (Figure 5a). Large increases in EVI occurred in areas with large increases in percent tree cover. EVI exhibited small or no increases in the majority of the remaining areas. The average EVI of the Loess Plateau significantly increased from 2000 to 2013 (Figure 5b; $y = 0.09x - 16.04$, $R^2 = 0.56$, $p < 0.01$). Over the 14 year period, the average growing season EVI increased by 0.12, with an increase of 6.6%.

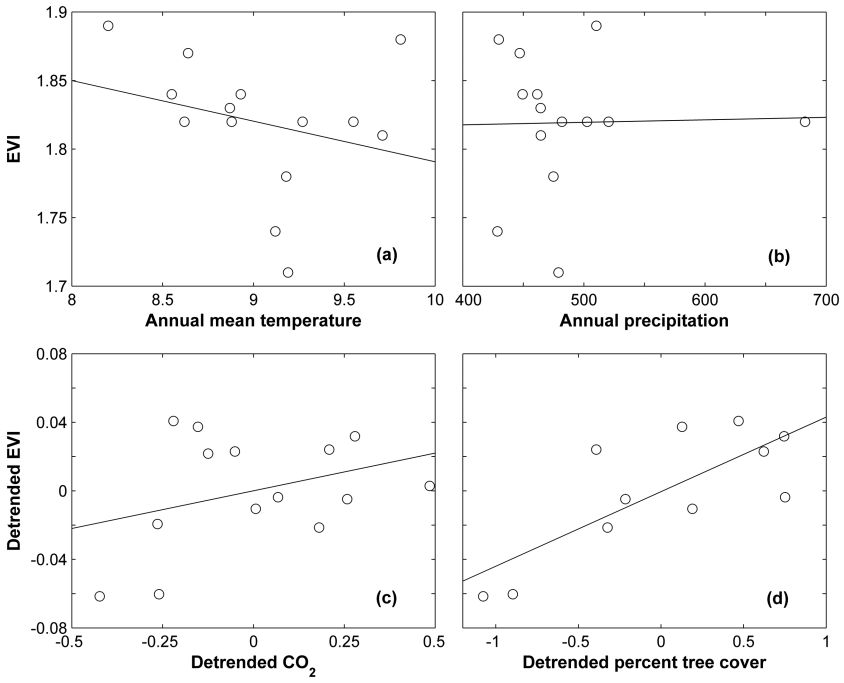

Figure 6. Relationships of growing season integrated EVI with (a) annual mean temperature, (b) annual precipitation, (c) atmospheric CO_2 concentrations, and (d) percent tree cover for the Loess Plateau. EVI, temperature, precipitation, and percent tree cover were averaged across the plateau. For Figures 6c and 6d, both EVI and CO_2 (or tree cover) were detrended.

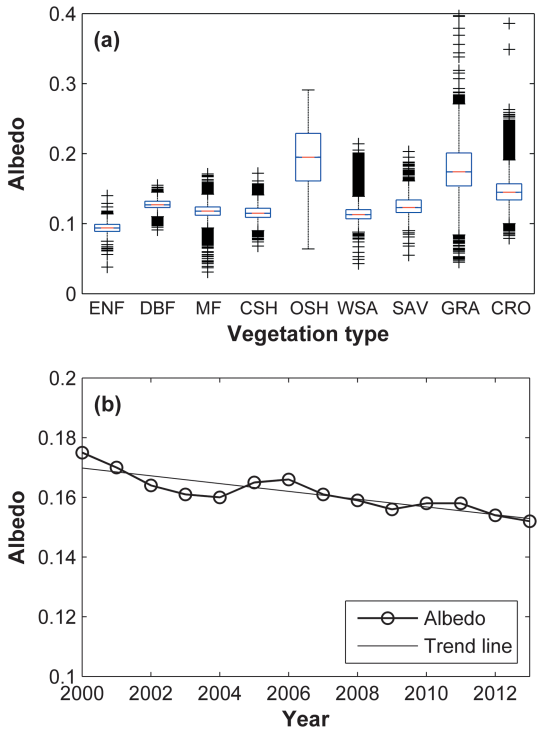

Figure 7. Albedo over the growing season of the Loess Plateau: (a) box plot of per pixel albedo in 2001 for each vegetation type; (b) the trend of the albedo averaged across the plateau from 2000 to 2013. The abbreviations for the vegetation types are spelled out in the caption of Figure 1.

Similarly, large increases in growing season mean LAI and fPAR occurred in eastern, southeastern, and southern Loess Plateau where large increases in percent tree cover and EVI were observed (Figures 5c and 5e). Averaged across the plateau, both LAI (Figure 5d; $y = 0.009x - 16.24$, $R^2 = 0.64$, $p < 0.001$) and fPAR (Figure 5f; $y = 0.007x - 13.50$, $R^2 = 0.64$, $p < 0.001$) exhibited significant increasing trends over the period 2000–2013. The LAI and fPAR averaged across the plateau increased by 0.11 and 0.09 over the 14 year period, respectively.

The relationships of the spatially averaged EVI with temperature, atmospheric CO_2 concentrations, and percent tree cover were examined using statistical analysis (Figure 6). Over the period 2000–2013, growing season integrated EVI was not significantly correlated with annual mean temperature (Figure 6a; $p = 0.34$). Similarly, EVI was not significantly related to annual precipitation (Figure 6b; $p = 0.94$). There was a strong relationship between EVI and atmospheric CO_2 concentrations. However, the detrending of the two variables destroyed the relationship, and there was no significant relationship between detrended EVI and detrended atmospheric CO_2 concentrations (Figure 6c; $p = 0.23$). By contrast, there was a strong relationship between EVI and percent tree cover

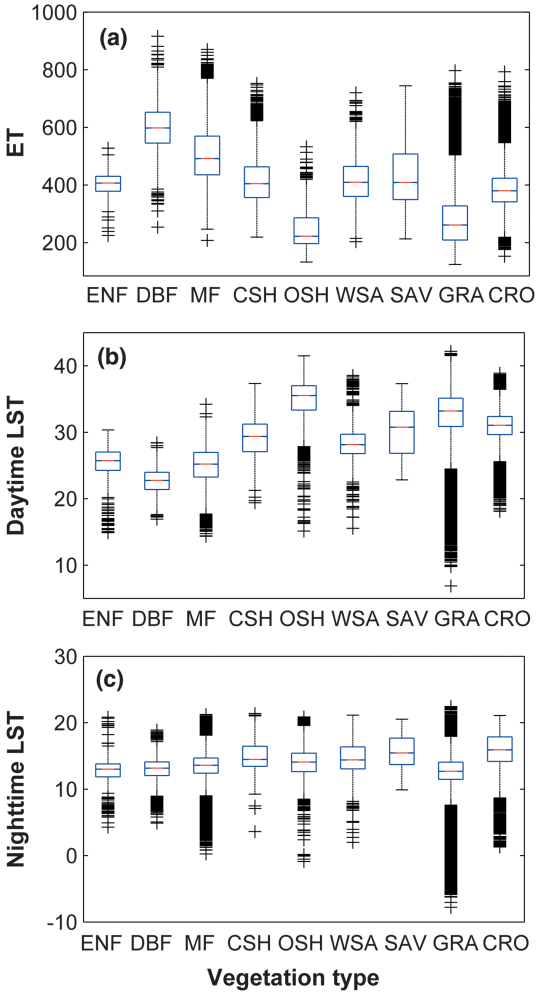

Figure 8. Box plots of per pixel ET, daytime LST, and nighttime LST for the Loess Plateau: (a) annual ET (mm yr^{-1}); (b) daytime LST (°C) averaged over the growing season; (c) nighttime LST (°C) averaged over the growing season. The abbreviations for the vegetation types are spelled out in the caption of Figure 1.

($y = 0.04x + 1.47$; $R^2 = 0.72$, $p < 0.001$); after detrending, EVI was still strongly correlated with percent tree cover (Figure 6d; $y = 0.04x - 0.0005$; $R^2 = 0.58$, $p < 0.01$).

3.3. Changes in Albedo and LST

The distribution of per pixel growing season mean albedo in 2001 for each vegetation type was illustrated in Figure 7a. Open shrublands had the highest albedo, followed by grasslands. Each forest type had lower albedo than croplands ($p < 0.0001$), indicating that the conversion of croplands to forests can result in the decrease in albedo. Among forests, evergreen needleleaf forests had lower albedo than deciduous broadleaf forests, indicating that the conversion of croplands to evergreen needleleaf forests can lead to lower albedo and have a larger cooling effect than the conversion of croplands to deciduous broadleaf forests. The albedo averaged across the plateau significantly declined over the period from 2000 to 2013 (Figure 7b; $y = -0.001x + 2.78$; $R^2 = 0.77$, $p < 0.001$). Over the 14 year period, the average albedo decreased from 0.17 to 0.15 with a relative decrease of 11.7%.

The distributions of per pixel annual ET and growing season mean daytime and nighttime LST in 2001 for the major vegetation type were summarized in Figure 8. Evergreen needleleaf forests had slightly higher ET than croplands ($p < 0.0001$), while deciduous broadleaf forests ($p < 0.0001$) and mixed forests ($p < 0.0001$) had much higher ET than croplands (Figure 8a). Forests had lower daytime LST than other vegetation types, and the difference between each forest type and cropland was statistically significant ($p < 0.0001$) (Figure 8b). This indicates that the conversion of croplands to forests resulting from the GGP can reduce daytime LST because of enhanced ET. By contrast, nighttime LST exhibited much smaller differences among vegetation types, and each forest type had slightly lower nighttime LST than croplands ($p < 0.0001$) (Figure 8c).

Daytime LST averaged over the growing season declined in many areas of the Loess Plateau over the period 2000–2013 (Figure 9a). Large decreases in daytime LST occurred in the areas with large increases in tree cover, EVI, LAI, and fPAR. Averaged across the plateau, daytime LST exhibited a decreasing trend over the 14 year period (Figure 9b; $y = -0.13x + 288.22$, $R^2 = 0.38$, $p < 0.02$). By contrast, nighttime LST exhibited only slight decreases in some of the areas with increases in tree cover (Figure 9c). Averaged across the plateau, nighttime LST exhibited no significant trend over the 14 year period (Figure 9d; $p = 0.55$).

The albedo and percent tree cover averaged across the plateau were negatively correlated with each other over the period 2000–2013 (Figure 10a), indicating that the increase in tree cover resulting from the GGP led to the decrease in albedo. The daytime LST was also negatively correlated with percent tree cover (Figure 10b). This indicates that afforestation led to a decrease in daytime LST because of enhanced ET. There was no significant relationship between nighttime LST and percent tree cover (Figure 10c).

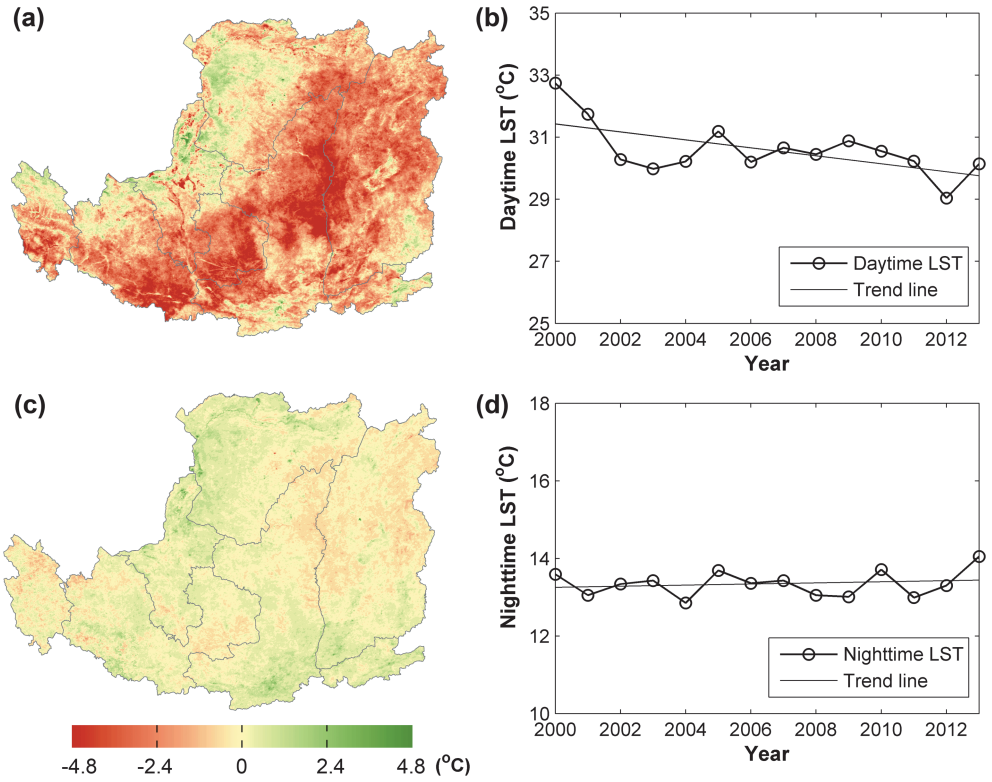

Figure 9. Trends of daytime and nighttime LST of the Loess Plateau over the period 2000–2013: (a) increases in daytime LST on a per pixel basis; (b) increase in average daytime LST of the plateau; (c) increases in nighttime LST on a per pixel basis; (d) increase in average nighttime LST of the plateau. The trends in Figures 9a and 9c are provided as increases in daytime and nighttime LST (°C) over the 14 year period.

4. Discussion

Both satellite-derived continuous fields and forestry statistics showed that tree cover on the Loess Plateau substantially increased since the launch of the GGP in 1999. This indicates that the effort in converting low-productivity croplands on steep slopes to forests has been generally effective. The GGP led to significant afforestation on the Loess Plateau, the pilot region of the program. It should be noted that the MODIS continuous field product [*DiMiceli et al.*, 2011] are likely to have significant uncertainty. Therefore, the direction of change in percent tree cover rather than its absolute magnitude is emphasized here.

The photosynthetic activity or vegetation productivity as approximated by EVI had significantly increased over the Loess Plateau. The trend analysis of EVI data indicated that the GGP resulted in significant increases in EVI in the northern Shaanxi from 1999 to 2005 [*H. J. Zhou et al.*, 2009]. Despite the changes in the climate of the Loess Plateau [*Wang et al.*, 2012], the increase in vegetation productivity was not correlated with elevated air temperature, changing precipitation, or rising atmospheric CO_2 concentrations. The strong correlation between EVI and percent tree cover indicated that the increase in vegetation productivity was driven by the increase in tree cover resulting from the GGP. Forests have higher GPP than croplands [*Xiao et al.*, 2013]. The conversion of croplands to forests can sequester carbon and has implications for the carbon cycle. The MODIS GPP/NPP data product is not suitable for assessing the effects of afforestation on carbon fluxes because this product does not account for the conversions of croplands to forests [*Zhao et al.*, 2005]. Previous modeling studies have shown that the GGP-enhanced carbon stocks in biomass and soils [*Chang et al.*, 2011; *Lu et al.*, 2012; *Liu et al.*, 2014] over the Loess Plateau.

Afforestation can alter the hydrological processes and surface energy exchange and have potentially significant feedbacks to the local and regional climate [*Bonan* 2008; *Y. Q. Liu et al.*, 2008]. The afforestation resulting from the GGP reduced the surface albedo of the Loess Plateau. The reduction of albedo can increase

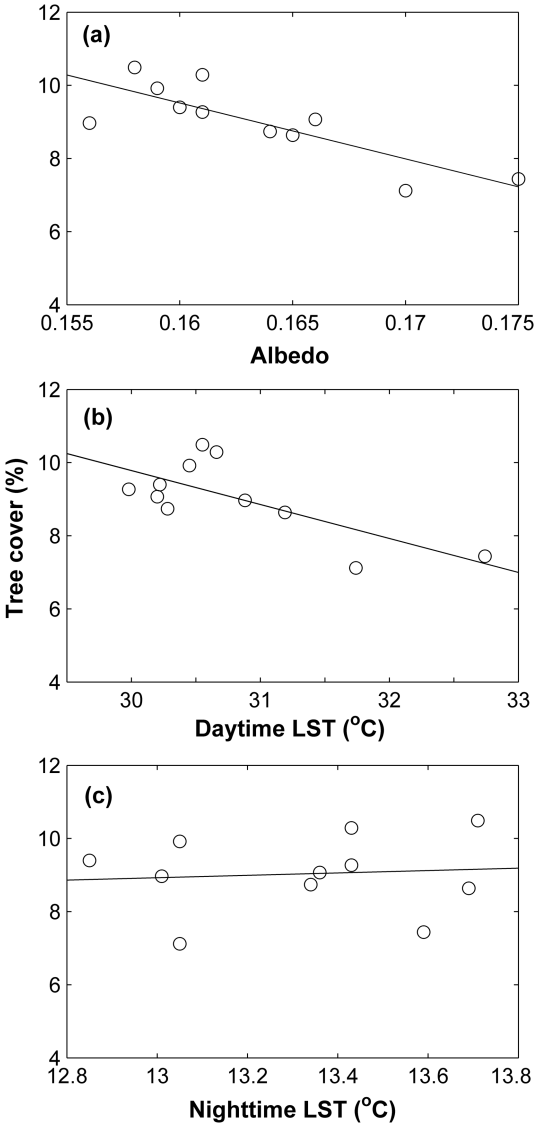

Figure 10. Relationships of percent tree cover (%) with (a) albedo, (b) daytime LST, and (c) nighttime LST averaged across the Loess Plateau.

the amount of solar radiation absorbed in the regional climate system, thereby having the potential to create a positive (heating) radiative forcing [*Betts*, 2000]. The positive forcing induced by decrease in albedo can offset the negative forcing from carbon sequestration to some extent [*Betts*, 2000].

Forests transpire more water than croplands during the daytime, leading to a cooling effect on forest canopies. Therefore, the afforestation reduced daytime surface temperature. In global climate models (GCMs), afforestation increases ET and surface roughness, leading to a local cooling effect [*Davin and de Noblet-Ducoudre*, 2010]. Deciduous broadleaf trees likely have stronger cooling effects than evergreen needleleaf trees [*Zhao and Jackson*, 2014]. Plants typically transpire a small amount of water during the night [*Tolk et al.*, 2006], and there are small differences in nighttime ET between forests and croplands [*Wickham et al.*, 2012]. The increase in forest cover therefore did not significantly decrease nighttime LST. The changes in latent heat flux resulting from afforestation can have local warming or cooling effects [*Davin and de Noblet-Ducoudre*, 2010; *Lee et al.*, 2011]. Therefore, better understanding of the influence of afforestation on ET has implications for quantifying the feedbacks of afforestation to the climate.

The afforestation can exert both positive and negative radiative forcing on the climate through its changes in albedo, ET, and surface roughness [*Brovkin et al.*, 2009]. These positive and negative effects can offset each other to some extent. The net radiative forcing of afforestation on the regional climate of the Loess Plateau depends on the offsetting of the negative forcing from carbon sequestration and higher ET and the positive forcing from lower albedo. Regional climate models that couple land surface models (e.g., Community Land Model or CLM) and atmospheric models such as RegCM5 are needed to quantify regional effects of afforestation by accounting for the land-atmosphere feedbacks [*Y. Q. Liu et al.*, 2008].

In addition to the biophysical consequences assessed in this study, the GGP also led to significant decreases in runoff and soil erosion of the Loess Plateau [*Deng et al.*, 2012; *Z. C. Zhou et al.*, 2009]. Large-scale afforestation has caused growing concerns for water supply and other ecosystem services [*Gao et al.*, 2014; *Jackson et al.*, 2005; *Sun et al.*, 2006]. The debates on afforestation effects on water balance are unsettled, and a mechanistic understanding of these effects is needed [*Mátyás and Sun*, 2014]. Mitigating soil erosion is an important goal of the GGP, and the decrease in soil erosion on the Loess Plateau [*Deng et al.*, 2012; *Feng et al.*, 2010; *Z. C. Zhou et al.*, 2009] can help conserve soil on the plateau and reduce the sediment loads in the Yellow River.

5. Conclusions

The analysis of a variety of MODIS data products showed that the Grain for Green Program has significant biophysical consequences for the Loess Plateau, the pilot region of the GGP. The GGP significantly increased

tree cover of the plateau. As a result, EVI, LAI, and fPAR significantly increased during the 14 year period from 2000 to 2013. The increase in forest productivity as approximated by EVI was not driven by elevated air temperature, changing precipitation, or rising atmospheric CO_2 concentrations. Afforestation reduced surface albedo and exerts a local warming effect. In the meanwhile, afforestation led to a significant decrease in daytime LST and exerts a local cooling effect. These positive and negative effects can offset each other to some extent. The feedbacks of the afforestation to the regional climate depend on the negative forcing from carbon sequestration and higher ET and the positive forcing from lower albedo. Regional climate models that couple land surface and atmospheric models and can account for the land-atmosphere feedbacks are needed to quantify the net effects of the GGP on the regional climate.

Acknowledgments

This work was financially supported by Nanjing University of Information Science and Technology and the U.S. National Science Foundation (NSF) through the MacroSystems Biology Program (award 1065777). The MODIS data products were obtained from NASA's Earth Observing System Data and Information System (EOSDIS; http://reverb.echo.nasa.gov). I would like to thank the PIs and other research personnel of the MODIS data products for developing these products and making them available to the research community, Dan Liu for providing the GIS data layer of the Loess Plateau, and Hongchun Peng and Shenghua Gao for obtaining the forestry statistics. I also thank the two anonymous reviewers for their constructive comments on the manuscript.

References

Asrar, G., M. Fuchs, E. T. Kanemasu, and J. L. Hatfield (1984), Estimating absorbed photosynthetic radiation and leaf-area index from spectral reflectance in wheat, *Agron. J.*, *76*(2), 300–306.

Betts, R. A. (2000), Offset of the potential carbon sink from boreal forestation by decreases in surface albedo, *Nature*, *408*(6809), 187–190, doi:10.1038/35041545.

Bonan, G. B. (2008), Forests and climate change: Forcings, feedbacks, and the climate benefits of forests, *Science*, *320*(5882), 1444–1449, doi:10.1126/science.1155121.

Brovkin, V., T. Raddatz, C. H. Reick, M. Claussen, and V. Gayler (2009), Global biogeophysical interactions between forest and climate, *Geophys. Res. Lett.*, *36*L07405, doi:10.1029/2009GL037543.

Chang, R. Y., B. J. Fu, G. H. Liu, and S. G. Liu (2011), Soil carbon sequestration potential for "Grain for Green" project in Loess Plateau, China, Environ, *Manage*, *48*(6), 1158–1172, doi:10.1007/s00267-011-9682-8.

Davin, E. L., and N. de Noblet-Ducoudre (2010), Climatic impact of global-scale deforestation: Radiative versus nonradiative processes, *J. Clim.*, *23*(1), 97–112, doi:10.1175/2009jcli3102.1.

Deng, L., Z. P. Shangguan, and R. Li (2012), Effects of the grain-for-green program on soil erosion in China, *Int. J. Sediment Res.*, *27*(1), 120–127.

Dickinson, R. E. (1995), Land processes in climate models, *Remote Sens. Environ.*, *51*(1), 27–38, doi:10.1016/0034-4257(94)00062-r.

DiMiceli, C. M., M. L. Carroll, R. A. Sohlberg, C. Huang, M. C. Hansen, and J. R. G. Townshend (2011), *Annual Global Automated MODIS Vegetation Continuous Fields (MOD44B) at 250 m Spatial Resolution for Data Years Beginning Day 65, 2000–2010, Collection 5 Percent Tree Cover*, Univ. of Maryland, College Park, Md.

Fang, J. Q., and Z. R. Xie (1994), Deforestation in preindustrial China—The Loess Plateau region as an example, *Chemosphere*, *29*(5), 983–999, doi:10.1016/0045-6535(94)90164-3.

Feng, X. M., Y. F. Wang, L. D. Chen, B. J. Fu, and G. S. Bai (2010), Modeling soil erosion and its response to land-use change in hilly catchments of the Chinese Loess Plateau, *Geomorphology*, *118*, 239–248, doi:10.1016/j.geomorph.2010.01.004.

Friedl, M. A., D. Sulla-Menashe, B. Tan, A. Schneider, N. Ramankutty, A. Sibley, and X. M. Huang (2010), MODIS Collection 5 global land cover: Algorithm refinements and characterization of new datasets, *Remote Sens. Environ.*, *114*(1), 168–182, doi:10.1016/j.rse.2009.08.016.

Gao, Y., X. J. Zhu, G. R. Yu, N. P. He, Q. F. Wang, and J. Tian (2014), Water use efficiency threshold for terrestrial ecosystem carbon sequestration in China under afforestation, *Agric. For. Meteorol.*, *195*, 32–37, doi:10.1016/j.agrformet.2014.04.010.

Hansen, M. C., R. S. DeFries, J. R. G. Townshend, R. Sohlberg, C. Dimiceli, and M. Carroll (2002), Towards an operational MODIS continuous field of percent tree cover algorithm: Examples using AVHRR and MODIS data, *Remote Sens. Environ.*, *83*(1–2), 303–319, doi:10.1016/s0034-4257(02)00079-2.

Hansen, M. C., S. V. Stehman, and P. V. Potapov (2010), Quantification of global gross forest cover loss, *Proc. Natl. Acad. Sci. U.S.A.*, *107*, 8650–8655, doi:10.1073/pnas.0912668107.

Huete, A., K. Didan, T. Miura, E. P. Rodriguez, X. Gao, and L. G. Ferreira (2002), Overview of the radiometric and biophysical performance of the MODIS vegetation indices, *Remote Sens. Environ.*, *83*(1–2), 195–213, doi:10.1016/s0034-4257(02)00096-2.

Jackson, R. B., E. G. Jobbagy, R. Avissar, S. B. Roy, D. J. Barrett, C. W. Cook, K. A. Farley, D. C. le Maitre, B. A. McCarl, and B. C. Murray (2005), Trading water for carbon with biological sequestration, *Science*, *310*, 1944–1947, doi:10.1126/science.1119282.

Justice, C. O., J. R. G. Townshend, E. F. Vermote, E. Masuoka, R. E. Wolfe, N. Saleous, D. P. Roy, and J. T. Morisette (2002), An overview of MODIS Land data processing and product status, *Remote Sens. Environ.*, *83*(1–2), 3–15, doi:10.1016/s0034-4257(02)00084-6.

Lawrence, P. J., and T. N. Chase (2007), Representing a new MODIS consistent land surface in the Community Land Model (CLM 3.0), *J. Geophys. Res.*, *112*, G01023, doi:10.1029/2006JG000168.

Lee, X., et al. (2011), Observed increase in local cooling effect of deforestation at higher latitudes, *Nature*, *479*(7373), 384–387, doi:10.1038/nature10588.

Liu, D., Y. Chen, W. W. Cai, W. J. Dong, J. F. Xiao, J. Q. Chen, H. C. Zhang, J. Z. Xia, and W. P. Yuan (2014), The contribution of China's grain to green program to carbon sequestration, *Landscape Ecol.*, *29*, 1675–1688, doi:10.1007/s10980-014-0081-4.

Liu, J. G., S. X. Li, Z. Y. Ouyang, C. Tam, and X. D. Chen (2008), Ecological and socioeconomic effects of China's policies for ecosystem services, *Proc. Natl. Acad. Sci. U.S.A.*, *105*, 9477–9482, doi:10.1073/pnas.0706436105.

Liu, X., J. Zhao, and X. Yu (2006), Climatic warming and drying trend and adaptation strategy of the Loess Plateau [in Chinese], *Arid Zone Res.*, *23*, 627–631.

Liu, Y. Q., J. Stanturf, and H. Q. Lu (2008), Modeling the potential of the Northern China forest shelterblet in improving hydroclimate conditions, *J. Am. Water Resour. Assoc.*, *44*(5), 1176–1192, doi:10.1111/j.1752-1688.2008.00240.x.

Lu, Y. H., B. J. Fu, X. M. Feng, Y. Zeng, Y. Liu, R. Y. Chang, G. Sun, and B. F. Wu (2012), A policy-driven large scale ecological restoration: Quantifying ecosystem services changes in the Loess Plateau of China, *PLoS One*, *7*, doi:10.1371/journal.pone.0031782.

Lyons, E. A., Y. F. Jin, and J. T. Randerson (2008), Changes in surface albedo after fire in boreal forest ecosystems of interior Alaska assessed using MODIS satellite observations, *J. Geophys. Res.*, *113*, G02012, doi:10.1029/2007JG000606.

Mátyás, C., and G. Sun (2014), Forests in a water limited world under climate change, *Environ. Res. Lett.*, *9*085001, doi:10.1088/1748-9326/9/8/085001.

Monteith, J. L. (1972), Solar-radiation and productivity in tropical ecosystems, *J. Appl. Ecol.*, *9*(3), 747–766, doi:10.2307/2401901.

Monteith, J. L. (1977), Climate and efficiency of crop production in Britain, *Philos. Trans. R. Soc. Lond. Ser. B-Biol. Sci.*, *281*(980), 277–294, doi:10.1098/rstb.1977.0140.

Mu, Q., F. A. Heinsch, M. Zhao, and S. W. Running (2007), Development of a global evapotranspiration algorithm based on MODIS and global meteorology data, *Remote Sens. Environ.*, *111*, 519–536, doi:10.1016/j.rse.2007.04.015.
Myneni, R. B., et al. (2002), Global products of vegetation leaf area and fraction absorbed PAR from year one of MODIS data, *Remote Sens. Environ.*, *83*(1–2), 214–231, doi:10.1016/s0034-4257(02)00074-3.
Pan, Y. D., et al. (2011), A large and persistent carbon sink in the world's forests, *Science*, *333*, 988–993, doi:10.1126/science.1201609.
Ren, M. E., and Y. L. Shi (1986), Sediment discharge of the Yellow-River (China) and its effect on the sedimentation of the Bohai and the Yellow Sea, *Cont. Shelf Res.*, *6*(6), 785–810, doi:10.1016/0278-4343(86)90037-3.
Rienecker, M. M., et al. (2011), MERRA: NASA's Modern-Era Retrospective Analysis for Research and Applications, *J. Clim.*, *24*, 3624–3648, doi:10.1175/jcli-d-11-00015.1.
Running, S. W., R. R. Nemani, F. A. Heinsch, M. S. Zhao, M. Reeves, and H. Hashimoto (2004), A continuous satellite-derived measure of global terrestrial primary production, *BioScience*, *54*, 547–560, doi:10.1641/0006-3568(2004)054[0547:acsmog]2.0.co;2.
Schaaf, C. B., et al. (2002), First operational BRDF, albedo nadir reflectance products from MODIS, *Remote Sens. Environ.*, *83*(1–2), 135–148, doi:10.1016/s0034-4257(02)00091-3.
Sims, D. A., et al. (2006), On the use of MODIS EVI to assess gross primary productivity of North American ecosystems, *J. Geophys. Res.*, *111*, G04015, doi:10.1029/2006JG000162.
State Forestry Administration of China (1977), *National Forest Resources Statistics (1973–1976)* [in Chinese], pp. 22–23, China Forestry Publishing House, Beijing.
State Forestry Administration of China (2000), *China Forestry Statistical Yearbook 1999* [in Chinese], 783 pp., China Forestry Publishing House, Beijing.
State Forestry Administration of China (2001), *China Forestry Statistical Yearbook 2000* [in Chinese], 762 pp., China Forestry Publishing House, Beijing.
State Forestry Administration of China (2002), *China Forestry Statistical Yearbook 2001* [in Chinese], 663 pp., China Forestry Publishing House, Beijing.
State Forestry Administration of China (2003), *China Forestry Statistical Yearbook 2002* [in Chinese], 749 pp., China Forestry Publishing House, Beijing.
State Forestry Administration of China (2004), 643 pages, *China Forestry Statistical Yearbook 2003* [in Chinese], China Forestry Publishing House, Beijing.
State Forestry Administration of China (2005), *China Forestry Statistical Yearbook 2004* [in Chinese], 570 pp., China Forestry Publishing House, Beijing.
State Forestry Administration of China (2006), *China Forestry Statistical Yearbook 2005* [in Chinese], 594 pp., China Forestry Publishing House, Beijing.
State Forestry Administration of China (2007), *China Forestry Statistical Yearbook 2006* [in Chinese], 584 pp., China Forestry Publishing House, Beijing.
State Forestry Administration of China (2008), *China Forestry Statistical Yearbook 2007* [in Chinese], 580 pp., China Forestry Publishing House, Beijing.
State Forestry Administration of China (2009a), *China Forest Resources Report—The Seventh National Forest Resources Inventory* [in Chinese], pp. 62–63.
State Forestry Administration of China (2009b), *China Forestry Statistical Yearbook 2008* [in Chinese], 496 pp., China Forestry Publishing House, Beijing.
State Forestry Administration of China (2010), *China Forestry Statistical Yearbook 2009* [in Chinese], 498 pp., China Forestry Publishing House, Beijing.
State Forestry Administration of China (2011), *China Forestry Statistical Yearbook 2010* [in Chinese], 498 pp., China Forestry Publishing House, Beijing.
State Forestry Administration of China (2012), *China Forestry Statistical Yearbook 2011* [in Chinese], 468 pp., China Forestry Publishing House, Beijing.
State Forestry Administration of China (2013), *China Forestry Statistical Yearbook 2012* [in Chinese], 452 pp., China Forestry Publishing House, Beijing.
Su, C. H., and B. J. Fu (2013), Evolution of ecosystem services in the Chinese Loess Plateau under climatic and land use changes, *Global Planet. Change*, *101*, 119–128, doi:10.1016/j.gloplacha.2012.12.014.
Sun, G., G. Y. Zhou, Z. Q. Zhang, X. H. Wei, S. G. McNulty, and J. M. Vose (2006), Potential water yield reduction due to forestation across China, *J. Hydrol.*, *328*, 548–558, doi:10.1016/j.jhydrol.2005.12.013.
Tolk, J. A., T. A. Howell, and S. R. Evett (2006), Nighttime evapotranspiration from alfalfa and cotton in a semiarid climate, *Agron. J.*, *98*, 730–736, doi:10.2134/agronj2005.0276.
Wan, Z. M., Y. L. Zhang, Q. C. Zhang, and Z. L. Li (2002), Validation of the land-surface temperature products retrieved from Terra moderate resolution imaging spectroradiometer data, *Remote Sens. Environ.*, *83*(1–2), 163–180, doi:10.1016/s0034-4257(02)00093-7.
Wang, Q. X., X. H. Fan, Z. D. Qin, and M. B. Wang (2012), Change trends of temperature and precipitation in the Loess Plateau Region of China, 1961–2010, *Global Planet. Change*, *92–93*, 138–147, doi:10.1016/j.gloplacha.2012.05.010.
Wickham, J. D., T. G. Wade, and K. H. Riitters (2012), Comparison of cropland and forest surface temperatures across the conterminous United States, *Agric. For. Meteorol.*, *166*, 137–143, doi:10.1016/j.agrformet.2012.07.002.
Xiao, J., and A. Moody (2005), Geographical distribution of global greening trends and their climatic correlates: 1982–1998, *Int. J. Remote Sens.*, *26*, 2371–2390, doi:10.1080/01431160500033682.
Xiao, J. F., and A. Moody (2004), Trends in vegetation activity and their climatic correlates: China 1982 to 1998, *Int. J. Remote Sens.*, *25*, 5669–5689, doi:10.1080/01431160410001735094.
Xiao, J. F., et al. (2008), Estimation of net ecosystem carbon exchange for the conterminous United States by combining MODIS and AmeriFlux data, *Agric. For. Meteorol.*, *148*, 1827–1847, doi:10.1016/j.agrformet.2008.06.015.
Xiao, J. F., et al. (2013), Carbon fluxes, evapotranspiration, and water use efficiency of terrestrial ecosystems in China, *Agric. For. Meteorol.*, *182–183*, 76–90, doi:10.1016/j.agrformet.2013.08.007.
Zhang, B. Q., P. T. Wu, X. N. Zhao, Y. B. Wang, J. W. Wang, and Y. G. Shi (2012), Drought variation trends in different subregions of the Chinese Loess Plateau over the past four decades, *Agric. Water Manage.*, *115*, 167–177, doi:10.1016/j.agwat.2012.09.004.
Zhao, K. G., and R. B. Jackson (2014), Biophysical forcings of land-use changes from potential forestry activities in North America, *Ecol. Monogr.*, *84*, 329–353, doi:10.1890/12-1705.1.
Zhao, M. S., F. A. Heinsch, R. R. Nemani, and S. W. Running (2005), Improvements of the MODIS terrestrial gross and net primary production global data set, *Remote Sens. Environ.*, *95*, 164–176, doi:10.1016/j.rse.2004.12.011.

Zheng, F. L. (2006), Effect of vegetation changes on soil erosion on the Loess Plateau, *Pedosphere*, *16*, 420–427, doi:10.1016/s1002-0160(06)60071-4.

Zheng, F. L., X. B. He, X. T. Gao, C. Zhang, and K. L. Tang (2005), Effects of erosion patterns on nutrient loss following deforestation on the Loess Plateau of China, *Agric. Ecosyst. Environ.*, *108*, 85–97, doi:10.1016/j.agee.2004.12.009.

Zhou, H. J., A. Van Rompaey, and J. A. Wang (2009), Detecting the impact of the "Grain for Green" program on the mean annual vegetation cover in the Shaanxi province, China using SPOT-VGT NDVI data, *Land Use Pol.*, *26*, 954–960, doi:10.1016/j.landusepol.2008.11.006.

Zhou, L. M., C. J. Tucker, R. K. Kaufmann, D. Slayback, N. V. Shabanov, and R. B. Myneni (2001), Variations in northern vegetation activity inferred from satellite data of vegetation index during 1981 to 1999, *J. Geophys. Res.*, *106*(D17), 20,069–20,083, doi:10.1029/2000JD000115.

Zhou, Z. C., Z. T. Gan, Z. P. Shangguan, and Z. B. Dong (2009), China's grain for green program has reduced soil erosion in the upper reaches of the Yangtze River and the middle reaches of the Yellow River, *Int. J. Sustain. Dev. World Ecol.*, *16*, 234–239, doi:10.1080/13504500903007931.